THE STRUCTURE OF PASSIVE SCALAR PLUMES IN TURBULENT BOUNDARY LAYERS

John P. Crimaldi*
Department of Civil, Environmental, and Architectural Engineering
University of Colorado at Boulder
428 UCB, Boulder, Colorado, USA 80309-0428
john.crimaldi@colorado.edu

Jeffrey R. Koseff
Department of Civil and Environmental Engineering
Stanford University
Stanford, California, USA 94305-4020

ABSTRACT

We present results of an experimental investigation of the temporal and spatial structure of a scalar plume developing within a turbulent boundary layer over a smooth bed. The source of the scalar plume is located flush with the bed, and the vertical momentum associated with the scalar release is extremely small. The source design is intended to simulate a diffusive-type scalar release. Planar laser-induced fluorescence (PLIF) and single-point laser-induced fluorescence (LIF) techniques were used to capture the spatial and temporal structure of the plume at resolutions of 150 μm and 2000 Hz, respectively. We present data that describes the characteristics of the mean and fluctuating scalar fields, including the scalar intermittency and the probability density function (pdf) of scalar differences. The results show a strong vertical variation in the plume structure typical of boundary layer flows.

INTRODUCTION

Scalar plumes developing in turbulent boundary layer flows are ubiquitous in both natural and engineered systems. Our primary motivation for studying scalar plumes is to develop insight into how animals make use of scalar structure in odor plumes to make inferences about the location of the plume source. This insight will ultimately be useful for designing search algorithms for autonomous robots that could locate the hidden source of plumes emanating from potentially dangerous sources.

Optical techniques such as planar laser-induced fluorescence (PLIF) provide detailed data on scalar structure in turbulent flows that reveals exciting visual insight into the structure of both the passive scalar as well as the underlying velocity field. The PLIF image in

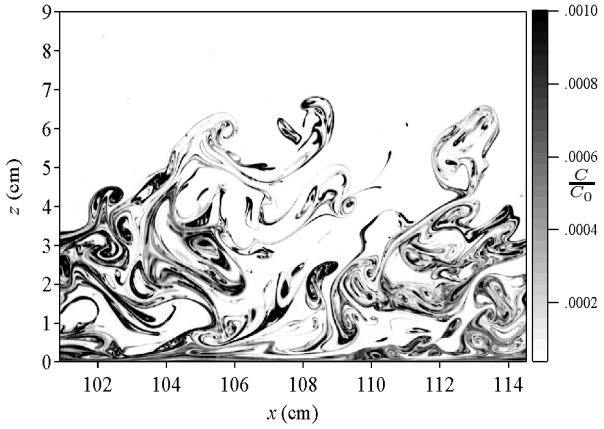

Figure 1: Image of the instantaneous normalized concentration structure in a thin vertical slice through the centerline of a scalar plume developing in a turbulent boundary layer. The scalar source is at $x = 0$, $z = 0$. Flow is from left to right.

Fig. 1 details the instantaneous spatial scalar structure in a thin vertical slice through the centerline of a plume. Turbulent boundary layer features such as bursts and sweeps as well as the viscous sublayer are visible in the image. In this paper we present the results of a statistical analysis performed on long series of such images.

Recent studies that used related PLIF techniques include Koochesfahani and Dimotakis

*This work was supported by the Office of Naval Research's Chemical Plume Tracing Program (Program Officer: Keith Ward), under Grants N00014-97-1-0706, N00014-98-1-0785, and N00014-00-1-0794. The authors are grateful to Meg Wiley for her assistance with the data collection.

(1985), Dahm et al. (1991), Brungart et al. (1991), Houcine et al. (1996), and Ferrier et al. (1993). Webster et al. (2001) used the PLIF technique to investigate bilateral correlations in turbulent odor plumes. A second technique used in the current study, a single-point LIF probe, was used to make high-resolution measurements of temporal scalar structure. Related approaches have been described by Durst and Schmitt (1984), Walker (1987), and Lemoine et al. (1999).

There are a number of existing studies involving plume structure from a variety of different source types. Two studies involving neutrally buoyant plumes released from ground-level sources into turbulent boundary layers are particularly relevant to the current study. Fackrell and Robins (1982) used a flame ionization system to study plumes released from various heights in a wind tunnel. Bara et al. (1992) used a conductivity probe to study plumes over rough surfaces in a water flume. In both of these studies, the source release involves a significant amount of (horizontal) momentum, and the release is distributed over a large (relative to the inner boundary layer scales) vertical distance. Shlien and Corrsin (1976) performed a study with a thermal release from a long thin heated wire located at the wall (and other locations), but presents only mean temperature results. Several analytical and numerical studies are also relevant to the current study: Robins (1978), El Tahry et al. (1981), and Hanna (1984) all discuss the statistics of scalar dispersal in turbulent boundary layers.

In the present study we investigate the scalar structure of a neutrally buoyant plume in a turbulent boundary layer. The plume emanates from a circular source region that is flush with the bed, and the momentum associated with the scalar release velocity is extremely low. The source geometry is designed to mimic a diffusive scalar release from a source that is buried below a smooth substrate. To our knowledge, the structure of plumes resulting from this type of source geometry have not been previously reported in the literature.

EXPERIMENTAL DETAILS

The experiments were conducted in the Environmental Fluid Mechanics Laboratory at Stanford University in a recirculating water flume with a glass-walled test section that is 3 m long and 0.6 m wide. Data were acquired at freestream velocities of 10 cm/s and 30 cm/s. The bed of the test section is smooth, and a 3 mm boundary layer trip is located at the upstream end. The flow depth in the test section was approximately 0.25 m. A schematic of the flume test section, showing the scalar source and the imaging apparatus, is given in Fig. 2.

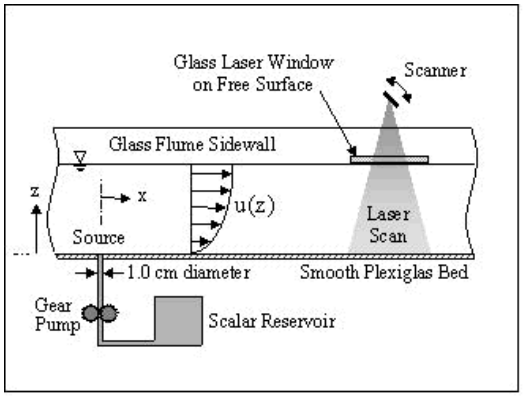

Figure 2: Side view of the flume test section showing the scalar source configuration and the imaging apparatus.

A passive scalar is introduced into the flow through the bed of the test section at $x = 0$. Rhodamine 6G in a 20 ppm aqueous solution is used as the scalar; Barrett (1989) reports the Prandtl number for the dye as 1250. The scalar source is located on the bed centerline, 2.2 m downstream of the turbulent boundary layer trip. The dye solution is pumped slowly through a 1 cm diameter circular hole drilled perpendicular to the bed in the floor of the flume. The hole is filled flush to the bed surface with a porous foam that is designed to provide uninterrupted boundary layer flow across the source exit. A small gear pump is used to pump the dye solution at a volumetric rate of 3 ml/ min, resulting in a vertical exit velocity of 0.063 cm/s. The electronic gear pump provides an accurate dose rate with no measurable pulsing.

The PLIF imaging apparatus consists of an argon-ion laser, optics for focusing and scanning the laser beam across the image area, and a 1024-by-1024 pixel, 12-bit greyscale digital camera. The laser optics and the camera can be positioned to allow imaging of the flow in either vertical or horizontal planes. For a typical 15 cm image size, the spatial pixel resolution is 150μm. The typical temporal exposure time of any give pixel is only 50μs. However, the PLIF framing rate for continuous acquisitions was limited to about 2 Hz. The PLIF image processing technique corrected the acquired images for variations in the laser scan intensity, fluorescence from the background dye concentration in the test section, quenching due to the background dye, as well as variations in the

optical path and in the CCD pixel response.

High temporal resolution scalar measurements were taken a discrete locations using a single point laser-induced fluorescence (LIF) probe. This probe used a photomultiplier tube in the backscatter optics of a laser-Doppler anemometer system to aquire 2000 Hz records of scalar fluctuations.

Details of the experimental facilities, the PLIF and LIF techniques, and the image processing algorithms are given by Crimaldi (2001).

RESULTS

Typical PLIF images of the instantaneous normalized scalar concentration field are shown in Fig. 1 (vertical slice) and Fig. 3 (horizontal slices). The concentrations are normalized by the source concentration C_0. The source is located at $x = y = z = 0$. The images in Fig. 3 are horizontal slices of the scalar field at two vertical locations, at the same streamwise location as Fig. 1. In Fig. 3(a), the image plane is located at $z^+ = 180$ (4 cm above the bed). The scalar typically reached this height via large coherent burst structures visible in Fig. 1. Scalar structures that reach this height persist for large advective distances, often with large regions of scalar-free fluid separating the structures. In Fig. 3(b), the image plane is located at $z^+ = 23$ (0.5 cm above the bed). The scalar structure is starting to exhibit the streakiness that is typical of the viscous wall region.

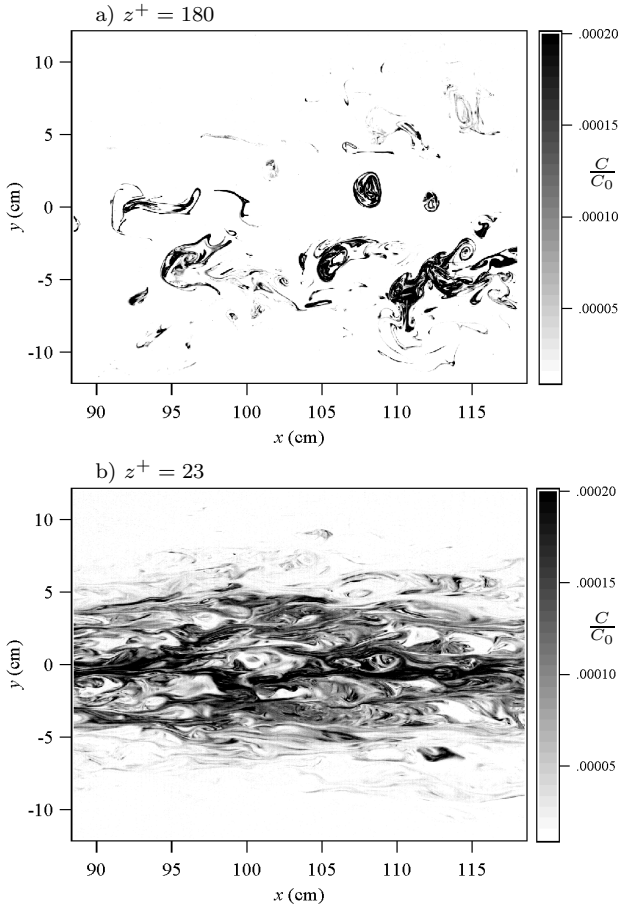

Figure 3: Image of the instantaneous normalized concentration structure in thin horizontal slices at $z^+ = 180$ (a) and $z^+ = 23$ (b). The scalar source is at $x = 0$, $z = 0$. Flow is from left to right.

Normalized lateral mean concentration profiles (calculated by averaging series of images such as those shown in Fig. 3) are shown in Fig. 4. Data for two flow speeds, five streamwise locations, and four vertical locations are shown. The data are normalized by the maximum local concentration C_m and the plume width σ_y, which were determined by fitting the data to the Gaussian curve

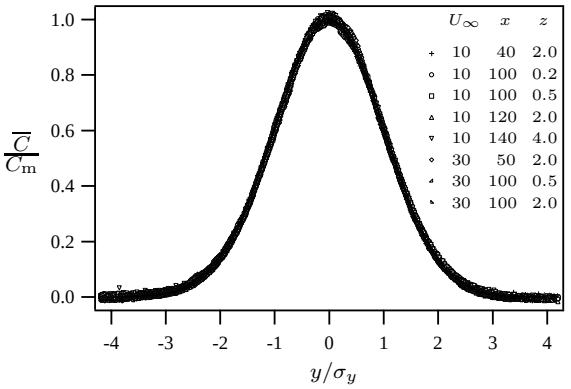

Figure 4: Normalized lateral profiles of mean concentration. Units in the legend are in terms of cm. The solid line is Eq. 1.

$$\overline{C}/C_\mathrm{m} = \exp(-y^2/2\sigma_y^2). \qquad (1)$$

The Gaussian is shown in Fig 4 by a solid line, although it is mostly hidden from view.

The two-dimensional lateral spreading rate for a plume released from a uniform vertical line source is

$$\sigma_y = \sqrt{\frac{2\epsilon_t}{\overline{u}}}x^{1/2}, \qquad (2)$$

where $\overline{u}$ is the depth-averaged velocity and ϵ_t is the lateral mixing coefficient. Various laboratory experiments in straight, rectangular open channels with smooth sides (but with a variety of bottom roughness types) have shown that the lateral mixing coefficient may be approximated as (Fischer et al. 1979)

$$\tilde{\epsilon_t} = 0.15 d u_\tau. \qquad (3)$$

where d is the flow depth and u_τ is the shear velocity. Using (3) as a baseline value for

the lateral mixing coefficient, we can write a general normalized expression for the lateral plume growth as

$$\frac{\sigma_y}{\sqrt{\frac{2\tilde{\epsilon}_t}{\overline{u}}}} = \sqrt{A}\,(x - x_0)^{1/2}\,, \qquad (4)$$

where we have included a offset distance x_0 from the source to the virtual plume origin at a given height, and where

$$A = \frac{\epsilon_t}{\tilde{\epsilon}_t}. \qquad (5)$$

Physically, x_0 is the streamwise location where the plume reaches a given distance from the bed (that is, x_0 is the location of the virtual plume origin at a given height). The ratio A indicates the degree to which Eq. 3 accurately models the lateral spreading rate. Streamwise distributions of the plume width σ_y were normalized using Eq. 4 with a two-parameter least-squares approach to determine x_0 and A. The resulting distributions for the 10 cm/s flow cases are shown in Fig. 5, along with the calculated A values. Since our boundary layer was not developed over the entire flow depth, the variables $\tilde{\epsilon}_t$ and $\overline{u}$ were calculated based on the boundary layer thickness δ instead of the flow depth d. The mixing

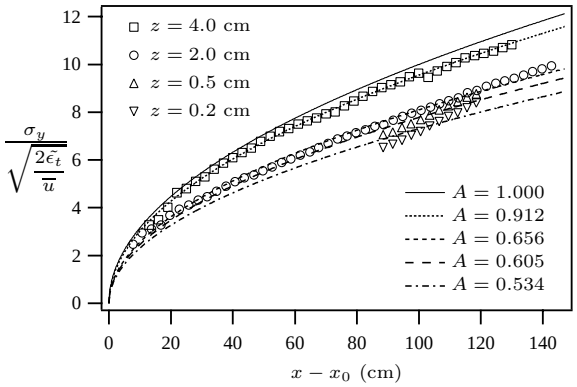

Figure 5: Normalized lateral plume growth as a function of downstream distance from the virtual plume origin for $U_\infty = 10$ cm/s.

coefficient approximation given by Eq. 3 accurately models the lateral spreading for data taken far from the bed at $z = 4.0$ cm (as witnessed by the near-unity value of A). Closer to the bed, however, the lateral mixing is suppressed: values of the lateral mixing coefficient as low as $0.534\tilde{\epsilon}_t$ were measured. The results show that the the lateral growth of the plume varies strongly with distance from the bed, and that a single depth-averaged value of the lateral mixing coefficient is not appropriate for three-dimensional plumes.

Normalized lateral profiles of the root-mean-square (rms) value of the concentration fluctuations c' where $c' = \langle c^2 \rangle^{1/2}$ are shown in Fig. 6. Again, the values of the normalization constants $c'_{\rm m}$ and σ_y were obtained using a fitting function given by the right-hand side of Eq. 1. Data from two flow conditions and multiple locations are included in the figure. The

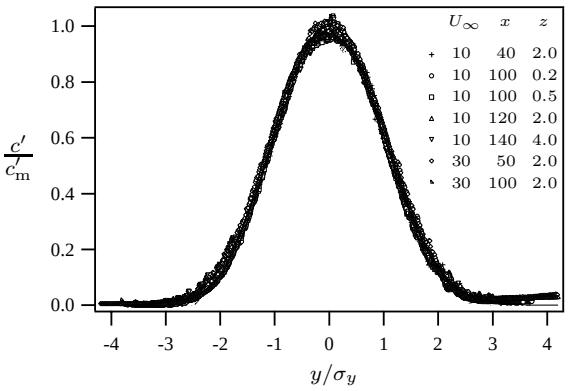

Figure 6: Normalized lateral profiles of rms concentration fluctuation strength. Units in the legend are in terms of cm. The solid line is the right-hand side of Eq. 1.

lateral profiles of c' are Gaussian, with no evidence of off-axis bipolar maxima, in contrast with data reported in several previous studies (Fackrell and Robins 1982; Bara et al. 1992). A meandering plume model developed by Bara et al. (1992) suggests that off-axis maxima occur only when the plume spreading is dominated by small-scale turbulent mixing rather than by mixing due to larger-scale meandering. Since the meandering scale becomes small relative to the plume width far from the source, the Bara model predicts that off axis maxima will occur at sufficiently large downstream distances.

Another statistical measure of the plume structure is the scalar intermittency, γ, defined herein as

$$\gamma = \text{prob}\,[C > C_T]\,, \qquad (6)$$

where C_T is a concentration threshold value; the choice of C_T involves some arbitrariness, as discussed in detail by Chatwin and Sullivan (1989). Nonetheless, a finite scalar threshold has physical significance for many problems. For the results presented here, we have chosen $C_T = 0.0002C_0$. Normalized lateral profiles of γ at $x = 100$ cm for three vertical locations for both flow cases are shown in Fig. 7. The values for $\gamma_{\rm m}$ and σ_y obtained by fitting $\gamma/\gamma_{\rm m}$ to the right-hand side of Eq. (1), which is included in the figure as a solid line. Also shown in the legend of the figure is the value of $\gamma_{\rm m}$ associated with each intermittency curve.

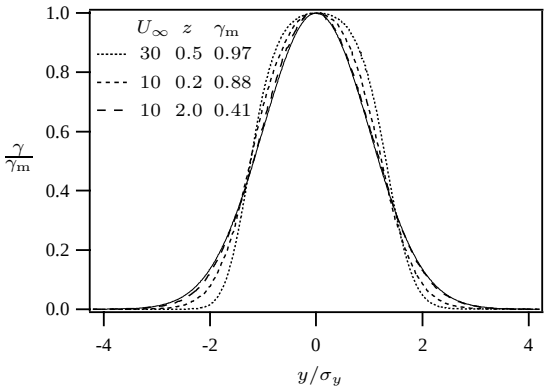

Figure 7: Normalized lateral profiles of concentration intermittency for $C_T = 0.002C_0$. Units in the legend are in terms of cm.

The shape of the lateral intermittency profile varies significantly with the vertical location in the flow. Close to the bed, where irreversible scalar mixing is more prevalent, the intermittency distribution tends away from the Gaussian shape towards a "top hat" profile, and $\gamma_m \rightarrow 1$. The scalar structure associated with this behavior is evident in the PLIF images in Fig. 3.

The turbulent scalar field is known to exhibit small-scale (internal) intermittency characterized by strong variability in the scalar dissipation ϵ_θ (Warhaft 2000). The statistics of ϵ_θ and hence of $\partial\theta/\partial t$ (which is often used as a surrogate for quantifying ϵ_θ) are therefore non-Gaussian. To investigate the statistics of $\partial\theta/\partial t$, we calculated the normalized scalar difference $\Delta\theta(r)/\Delta\theta'(r)$, where $\Delta\theta(r) = \theta(r) - \theta(0)$, r is a streamwise spatial separation, and $\Delta\theta' = \langle\Delta\theta^2\rangle^{\frac{1}{2}}$. In Fig 8, we plot the probability density function (pdf) of the normalized scalar differences for a separation difference $r = \mathcal{L}_\theta$ where $\mathcal{L}_\theta$ is the local scalar integral scale. Values for $\mathcal{L}_\theta$ were calculated by integrating the scalar autocorrelation function using long, 2000 Hz scalar records acquired with the LIF probe. Figure 8 contains pdfs calculated at three different vertical locations, all at $x = 100$ cm. A Gaussian is also shown in the figure for reference. The scalar difference is strongly non-Gaussian at all vertical locations in the flow, but most strongly at locations away from the bed where the intermittency is largest.

The degree of departure of the scalar difference pdf from the Gaussian can be quantified via the Kurtosis, K (where K=3 for a Gaussian). Figure 9 contains calculated values of K as a function of $r/\mathcal{L}_\theta$ for the same three vertical locations shown in Fig. 8. Note that K approaches a constant value for $r/\mathcal{L}_\theta > 1$,

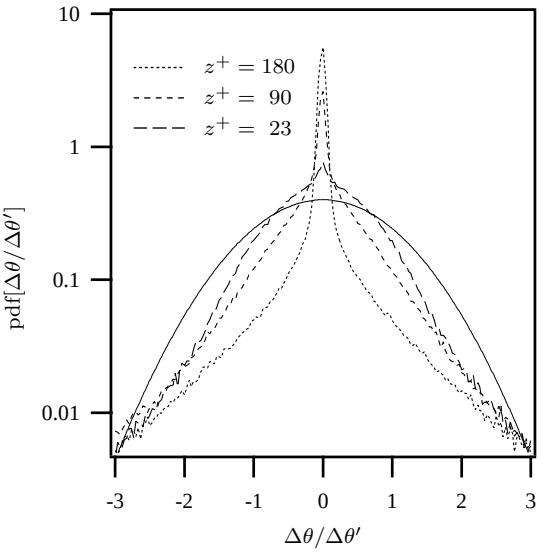

Figure 8: The probability density function (pdf) of the normalized scalar difference at a horizontal separation distance $r = \mathcal{L}_\theta$ for three vertical locations in the boundary layer. A Gaussian is shown (solid line) for comparison.

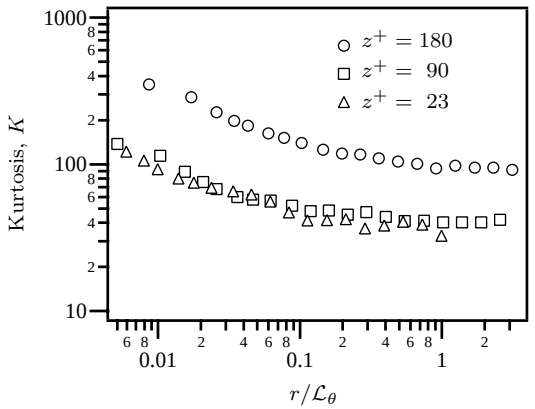

Figure 9: Kurtosis of the scalar difference as a function of the normalized distance $r/\mathcal{L}_\theta$ for the same locations as in Fig. 8.

but that $K >> 3$ for all values of r. This is in contrast to the DNS results (using a random velocity field) of Chen and Kraichnan (1998) that predict that $K \rightarrow 3$ as $r \rightarrow \mathcal{L}_\theta$. The implication here seems to be that the structure of the velocity field enhances the intermittency of the scalar field in real flows.

SUMMARY

The analysis of the LIF and PLIF scalar concentration data presented herein demonstrates the strong three-dimensionality of the scalar structure of plumes developing in turbulent boundary layers. As is typical of boundary layer statistics, the scalar structure variation is most pronounced in the direction normal to the bed. Many of the basic scalar statistics (e.g. the mean concentration and the rms concentration) exhibit Gaussian spatial distributions

in the lateral direction. Lateral profiles of the scalar intermittency, however, were shown to be non-Gaussian.

Small-scale (internal) intermittency results in non-Gaussian pdfs for statistics like $\partial\theta/\partial\, t$. The high Kurtosis of the scalar difference distributions provides evidence of high intermittency in the scalar dissipation and scalar mixing rates.

* REFERENCES

Bara, B., D. Wilson, and B. Zelt (1992). Concentration fluctutation profiles from a water channel simulation of a ground-level release. *Atmospheric Environment 26A*, 1053–1062.

Barrett, T. (1989). *Nonintrusive optical measurements of turbulence and mixing in a stably-stratified fluid*. Ph. D. thesis, University of California, San Diego.

Brungart, T., H. Petrie, W. Harbison, and C. Merkle (1991). A fluorescence technique for measurement of slot injected fluid concentration profiles in a turbulent boundary layer. *Experiments in Fluids 11*, 9–16.

Chatwin, P. and P. J. Sullivan (1989). The intermittency factor of scalars in turbulence. *Physics of Fluids A 4*, 761–763.

Chen, S. and R. Kraichnan (1998). Simulations of a randomly advected passive scalar field. *Physics of Fluids 10*, 2867–84.

Crimaldi (2001). High-resolution measurements of the spatial and temporal structure of a turbulent plume. *Experiments in Fluids*. In press.

Dahm, W. J., K. B. Southerland, and K. A. Buch (1991). Direct, high resolution, four-dimensional measurements of the fine scale structure of Sc$\gg$ 1 molecular mixing in turbulent flows. *Physics of Fluids A 3*, 1115–1127.

Durst, F. and F. Schmitt (1984). Joint laser-doppler/laser-induced fluorescence measurements in a turbulent jet. In *Proceedings of the 2nd Symposium on Applications of Laser Anemometry to Fluid Mechanics*.

El Tahry, S., A. Gosman, and B. Launder (1981). The two- and three-dimensional dispersal of a passive scalar in a turbulent boundary layer. *International Journal of Heat and Mass Transfer 24*, 35–46.

Fackrell, J. and A. Robins (1982). Concentration fluctuations and fluxes in plumes from point sources in a turbulent boundary layer. *Journal of Fluid Mechanics 117*, 1–26.

Ferrier, A., D. Funk, and P. Roberts (1993). Application of optical techniques to the study of plumes in stratified fluids. *Dynamics of Atmospheres and Oceans 20*, 155–183.

Fischer, H., E. List, R. Koh, J. Imberger, and N. Brooks (1979). *Mixing in Inland and Coastal Waters*. San Diego: Academic Press, Inc.

Hanna, S. (1984). Concentration fluctuations in a smoke plume. *Atmospheric Environment 18*, 1091–1106.

Houcine, I., H. Vivier, E. Plasari, and J. Villermaux (1996). Planar laser induced fluorescence technique for measurements of concentration in continuous stirred tank reactors. *Experiments in Fluids 22*, 95–102.

Koochesfahani, M. M. and P. E. Dimotakis (1985). Laser-induced fluorescence measurements of mixed fluid concentration in a liquid plane shear layer. *AIAA Journal 23*, 1700–1707.

Lemoine, F., Y. Antoine, M. Wolff, and M. Lebouche (1999). Simultaneous temperature and 2d velocity measurements in a turbulent heated jet using combined laser-induced fluorescence and LDA. *Experiments in Fluids 26*, 315–323.

Robins, A. (1978). Plume dispersion from ground level sources in simulated atmospheric boundary layers. *Atmospheric Environment 12*, 1033–1044.

Shlien, D. and S. Corrsin (1976). Dispersion measurements in a turbulent boundary layer. *Int. J. Heat Mass Transfer 19*, 285–295.

Walker, D. (1987). A fluorescence technique for measurement of concentration in mixing liquids. *J. Phys. E:Sci. Instrum. 20*, 217–224.

Warhaft, Z. (2000). Passive scalars in turbulent flows. *Annual Review of Fluid Mechanics 32*, 203–240.

Webster, D., S. Rahman, and L. Dasi (2001). On the usefulness of bilateral compar-

isons to tracking turbulent chemical odor plumes. *Limnology and Oceanography*. In press.